Quantitation of Tissue Resection Using a Brain Tumor Model and 7-T Magnetic Resonance Imaging Technology

Dan Huy Tran[1], Alexander Winkler-Schwartz[1], Marius Tuznik[2], Houssem-Eddine Gueziri[3], David A. Rudko[2,4], Aiden Reich[1], Recai Yilmaz[1], Bekir Karlik[1], D. Louis Collins[3], Adrian Del Maestro[5], Rolando Del Maestro[1]

■ BACKGROUND: **Animal brain tumor models can be useful educational tools for the training of neurosurgical residents in risk-free environments. Magnetic resonance imaging (MRI) technologies have not used these models to quantitate tumor, normal gray and white matter, and total tissue removal during complex neurosurgical procedures. This pilot study was carried out as a proof of concept to show the feasibility of using brain tumor models combined with 7-T MRI technology to quantitatively assess tissue removal during subpial tumor resection.**

■ METHODS: **Seven ex vivo calf brain hemispheres were used to develop the 7-T MRI segmentation methodology. Three brains were used to quantitate brain tissue removal using 7-T MRI segmentation methodology. Alginate artificial brain tumor was created in 4 calf brains to assess the ability of 7-T MRI segmentation methodology to quantitate tumor and gray and white matter along with total tissue volumes removal during a subpial tumor resection procedure.**

■ RESULTS: **Quantitative studies showed a correlation between removed brain tissue weights and volumes determined from segmented 7-T MRIs. Analysis of baseline and postresection alginate brain tumor segmented 7-T MRIs allowed quantification of tumor and gray and white matter along with total tissue volumes removed and detection of alterations in surrounding gray and white matter.**

■ CONCLUSIONS: **This pilot study showed that the use of animal tumor models in combination with 7-T MRI technology provides an opportunity to increase the granularity of data obtained from operative procedures and to improve the assessment and training of learners.**

INTRODUCTION

Surgical technical skills education is evolving from a time-focused apprenticeship toward a quantifiable competency-based model.[1] Competency in bimanual psychomotor performance in neurosurgery may be considered to have been achieved when the trainee can safely and efficiently perform a variety of procedures using appropriate surgical techniques.[2] The subpial resection procedure allows neurosurgeons to resect brain tumors and epileptic foci that border on important cortical structures and to minimize injury to adjacent pial-lined gyral tissues and hemorrhage from subpial vascular structures.[3,4] Maintaining pial layer integrity is associated with better postsurgical patient outcomes and is an important bimanual technical skill for surgical trainees to master.[3] Studies on virtual reality neurosurgical simulators with haptic feedback highlight the importance of quantitating performance of simulated subpial resection skills. Normal gray and white matter tissue along with tumor volume resection associated with subpial

Key words
- Alginate
- Brain tumors
- Ex vivo model
- MRI segmentation
- Quantitative MRI assessment
- Simulation

Abbreviations and Acronyms
3D: Three-dimensional
FOV: Field of view
MR: Magnetic resonance
MRI: Magnetic resonance imaging
ROI: Region of interest

From the [1]Neurosurgical Simulation and Artificial Intelligence Learning Centre, Department of Neurology and Neurosurgery, Montreal Neurological Institute, McGill University, Montreal, Quebec, Canada; [2]Department of Neurology/Neurosurgery, [3]Neuro Imaging and Surgical Technologies Laboratory, and [4]Quantitative Microstructure Imaging Laboratory, Department of Neurology/Neurosurgery and Department of Biomedical Engineering, McConnell Brain Imaging Centre, Montreal Neurological Institute, McGill University Montreal, Quebec, Canada; and [5]Department of Physics & Astronomy, Min H. Kao Department of Electrical Engineering and Computer Science, University of Tennessee, Knoxville, Tennessee, USA

To whom correspondence should be addressed: Dan Huy Tran, M.Sc. [E-mail: dan.h.tran@mail.mcgill.ca]

Citation: World Neurosurg. (2021) 148:e326-e339. https://doi.org/10.1016/j.wneu.2020.12.141

*Journal homepage: **www.journals.elsevier.com/world-neurosurgery***

*Available online: **www.sciencedirect.com***

resection, force application,[5-10] tool acceleration,[11] bimanual dexterity,[10,12-14] and impact of stress[14] have all been used to assess level of expertise on these simulators.[15] Linking neurosurgical psychomotor bimanual skill performance in virtual reality simulator scenarios to resident specific training in operating room environments continues to be challenging. There is a need to outline models that can accurately quantitate both technical psychomotor skills and operative results in realistic operative settings with comparable virtual reality simulator resident evaluations of similar scenarios. These models need to possess both visual and tactile reality and be coupled with advanced quantitation magnetic resonance imaging (MRI) methodology. An animal model allowing quantitative assessment of surgical performance during the subpial resection for tumor procedures would be an important adjuvant in competency-based surgical education. Analytical MRI protocols based on the comparative analysis of baseline and postoperative images of patients are common but do not allow quantitative assessments of psychomotor performance during complex procedures such as subpial resection.[16,17] Although automatic methods exist to carry out these studies, manual segmentation delimitating abnormal tissue contours is also used and remains the gold standard.[16,18,19] To make this method more efficient, semiautomatic tools exist that require decreased user input to perform these tasks.[20-25] These magnetic resonance (MR) technologies have not been used in animal models to quantitate normal gray and white matter removal to improve access for tumor resection along with resultant tissue injury. We have developed a framework whereby neurosurgical performance and extent of resection can be accurately quantified in a controlled setting using an ex vivo calf brain artificial alginate tumor model.[26] This framework allows manual and semiautomatic brain segmentations on baseline and postresection MRIs. Images are acquired on a 7-T MRI scanner to optimize image registration and to carry out quantitative analysis of normal tissue and brain tumor resected volumes during the use of the subpial technique.[26] The choice of 7-T MRI over 3-T MRI for its increased spatial resolution allowed for better resolution of subtle landmarks in brain tissue.[27,28] High spatial resolution was critical in producing accurate segmentation of MRIs, thus increasing the accuracy of the subsequent MRI registration. This pilot study was carried out as a proof of concept to show the feasibility of using brain tumor models combined with 7-T MRI technology with the aim of verifying that the union of these methodologies is both a feasible and practical application in the quantitation and understanding of complex neurosurgical skills.

The aims of this pilot study aims were 1) to determine if the assessment of baseline images and postresection images acquired using a 7-T MRI scanner can accurately quantitate normal brain tissue removed in a calf brain model; 2) to assess if baseline and postresection 7-T MRI technology can quantitate alginate brain tumor resected after subpial resection in a calf brain model; and 3) to outline if baseline and postresection 7-T MRI technology can quantitate gray matter, white matter, and total tissue resection after subtotal and total subpial resection of alginate brain tumor in a calf brain model. To our knowledge, this is the first study to use a brain tumor model and 7-T MRI technology to gain insight into quantification of specific tissue resection during a complex neurosurgical procedure.

METHODS

Ex Vivo Calf Brain Models

Seven fresh ex vivo calf brain cortical hemispheres were used for these studies because they structurally resemble human brain, are low cost, and are small enough (about 150 g) to fit into the 7-T MRI coil (**Figure 1A**).[26] The calf hemispheres were separated into 2 groups. Group 1 included 3 hemispheres that were used to assess if comparing baseline and postresection 7-T MRIs can quantitate normal brain tissue removed. Initial baseline scans were carried out before tissue resection (**Figure 1C**). Six brain segments of increasing sizes were resected from 3 calf hemispheres (**Figure 1B**). All resected brain segments were weighed (High Precision Scale [Smart Weight Ltd, Changzhou, China]). Calf hemispheres with resected segments then underwent a postresection scan (**Figure 1D**). In group 2, the cortical gray matter gyri of 4 calf hemispheres were used to create alginate artificial tumors of different sizes. Baseline 7-T scans were then carried out. After this scan, the neurosurgical resident operator was given specific instruction on how to perform a subpial resection of the overlying cortical gray matter tissue and tumor with minimal injury to underlying white matter tracts. After procedural completion, postresection scans were performed. Group 2 was used to assess if our pipeline of segmentation and registration of 7-T MRIs can quantitate percentage of alginate brain tumor resection and quantitate gray and white matter removed and total tissue resected during the subpial procedure in the calf model. The McGill University Health Centre Research Ethics Board, Neurosciences-Psychiatry approved these studies.

Image Acquisition Using a 7-T MRI Scanner

Before baseline scans, three-dimensional (3D)-printed polylactic acid fiducials were inserted into all 3 calf hemispheres in group 1 and 1 of 4 calf brains in group 2 (**Figure 2A** and **B**). The fiducials were used to assess their usefulness during registration of baseline and postresection images. Calf hemispheres were placed in a cylindrical container and covered with an MR-invisible fluorinated solution, FC-40 (Sigma Aldrich, St. Louis, Missouri, USA).

In this study, hydrogen 1 MR scans at a resonance frequency of 300 MHz were performed using a Bruker Pharmascan 7-T MRI scanner with an AVANCE II radiofrequency amplifier system and a BFG-150/90-S gradient system (Bruker Biosciences, Billerica, Massachusetts, USA). The plastic tubes containing the brain hemispheres were imaged inside a cylindrical radiofrequency transceiver coil with an inner diameter of 6 cm. The sequences were run using the Bruker proprietary imaging software ParaVision 5.1. For each brain hemisphere, the same scanning protocol was performed to obtain baseline MRIs and postresection MRIs.

All 3 brains of group 1 were scanned using a 3D fast imaging with steady-state free precession sequence with, echo time, 5 milliseconds; repetition time, 10 milliseconds; scan repetition time, 4000 milliseconds; receiver bandwidth, 50 kHz; flip angle, 30°; axial field of view (FOV), 6 × 5.25 × 5.1 cm; voxel resolution,

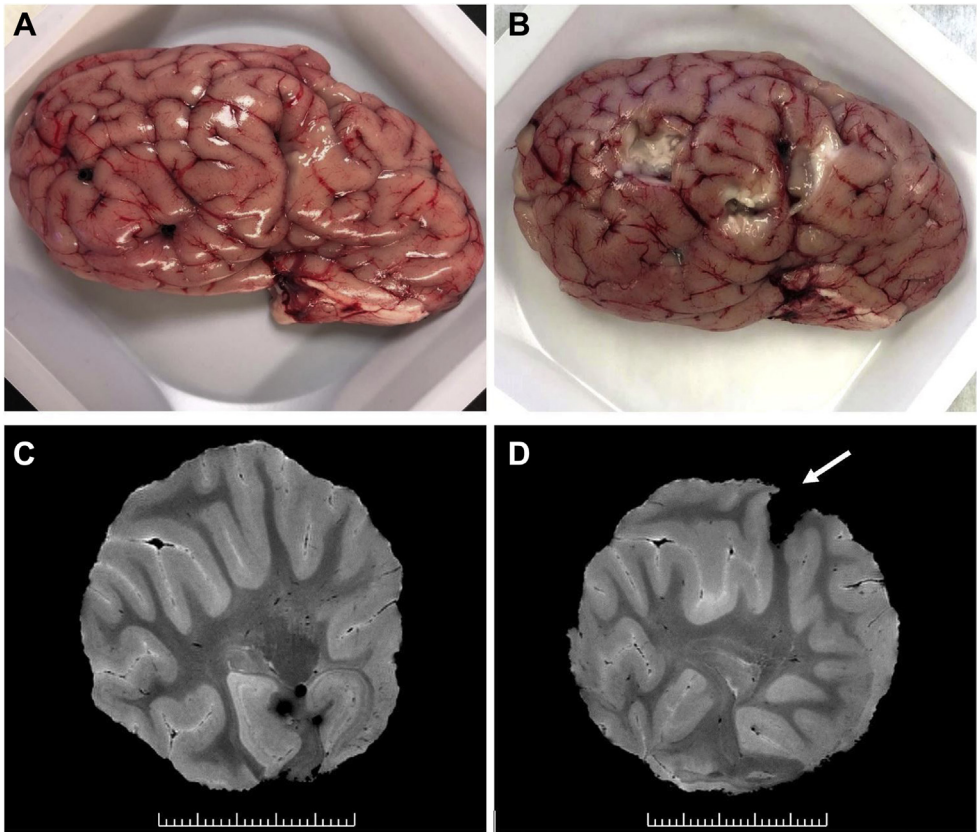

Figure 1. Calf brain from group 1. (**A**) Before resection of brain segments. (**B**) After resection of brain segments. (**C**) Coronal 7-T magnetic resonance imaging before segment resection (scale bar, 25 mm). (**D**) Coronal 7-T magnetic resonance imaging after resection showing area (*arrow*) of brain segment removed (scale bar, 25 mm).

200 μm; and matrix size, 300 × 255 × 255. Twenty-four averages were acquired, making for an anticipated total scan time of approximately 12 hours. Parameters were adjusted to determine the set of geometric parameters that represented the most optimal trade-off between spatial coverage and scan time. The parameters had to produce an FOV that encompassed the entire tumor in each brain and ensured that each scan did not exceed reasonable periods of time. All 4 brains of group 2 were scanned using a 3D fast imaging with steady-state free precession sequence with echo time of 5 milliseconds. The following parameters were common to all 4 brains of group 2: repetition time, 10 milliseconds; scan repetition time, 4000 milliseconds; receiver bandwidth, 50 kHz; and flip angle, 30°. The differences in protocol between the 4 brains included the FOV, matrix size, resolution, and antialiasing. The resolution for brains 1, 2, and 3 was 150 μm and the resolution for brain 4 was 200 μm: brain 1, axial FOV, 4.8 ×4.5 ×3.3 cm; matrix size, 320 × 300 × 220; brain 2, axial FOV, 5.25 ×5.25 ×3.3 cm; matrix size, 350 × 350 × 22; brain 3, sagittal FOV, 6 × 5.1 × 5.1 cm; matrix size, 300 × 255 × 255; brain 4, coronal FOV, 5.70 × 5.25× 2.64 cm; matrix size, 380 × 350 × 176.

Calf Brain Tumor Model

The created artificial tumor consisted of a 2% weight by volume Algin I-1G Alginate (KIMICA Corporation, Tokyo, Japan) and a calcium sulfate solution (final calcium concentration in the alginate 12 mM) along with a 10 times dilution of gadolinium solution, Gadobutrol (Bayer AG, Leverkusen, Germany) as previously described by Winkler-Schwartz et al.[26] Alginate tumor stiffness was optimized based on data obtained from human tumor samples and food coloring (Club House [McCormick & Company, Inc., Hunt Valley, Maryland, USA]) was added to simulate realistic brain tumor color. The alginate, calcium, and gadolinium mixture was injected at a subcortical depth of 5–7 mm into the gray matter of a cortical gyrus to standardize tumor location.[26] After baseline 7-T MR scan completion, the hemisphere was inserted into a plastic receptacle mimicking the shape of a human skull with surgical towels lining the surgical wound to replicate the human operating room environment. The gyrus region containing the tumor that was to be resected by the operator was outlined with black marker (Figure 2B). In an animal operative room, brain tumor resection was carried out using a subpial

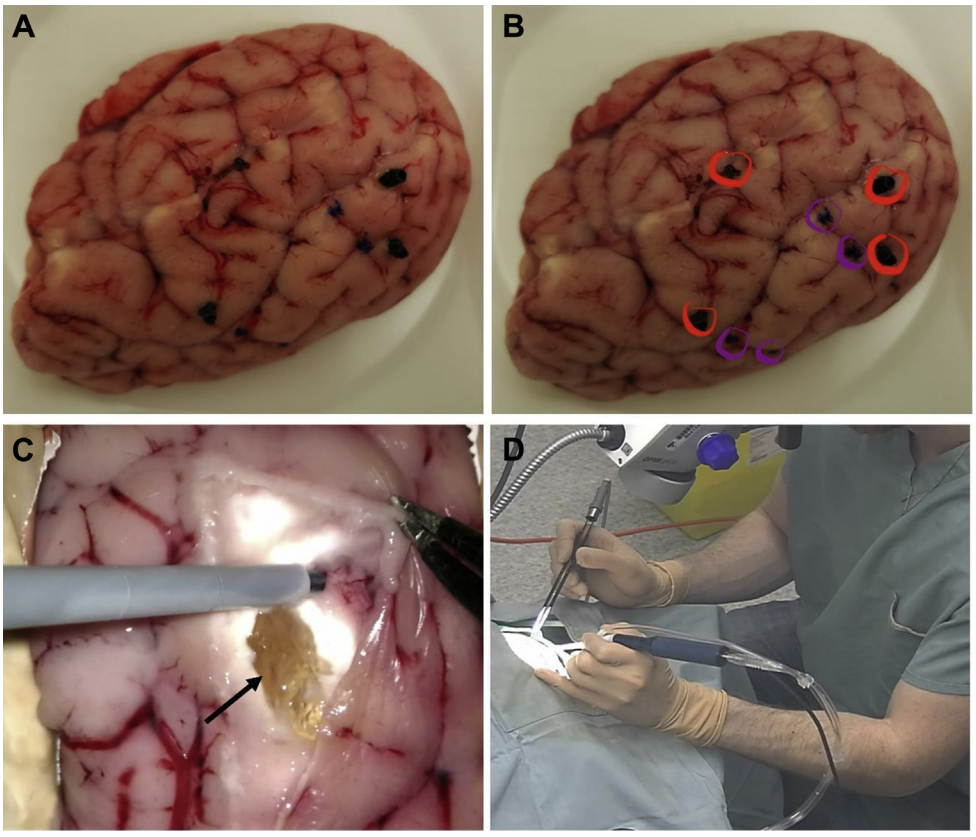

Figure 2. Calf brain hemisphere from group 2. (**A**) Inserted fiducials and markings outlining gyrus containing alginate tumor. (**B**) Fiducials are outlined in *red* and the gyrus to be resected containing tumor is between the marking outlined in *blue*. (**C**) View through the operating microscope showing the bipolar forceps holding the pia and ultrasonic aspirator being used to carry out a subpial gyral resection involving the gray matter overlying the visualized tumor (*arrow*). (**D**) Operator carrying out the subpial gyral resection and the tumor resection.

technique using microscissors to incise the pia mater, a bipolar coagulator to lift the pia and a Sonopet ultrasonic aspirator (Stryker, Kalamazoo, Michigan, USA), to remove normal cortical gray matter overlying and surrounding the artificial brain tumor visualized through an OPMI Pico surgical microscope (Carl Zeiss Co., Oberkochen, Germany) (**Figure 2C and D**). A sample operation of the subpial resection technique can be viewed in **Video 1** from Ref.26. After the operator judged that the tumor had been completely removed, the brain then underwent a postresection 7-T MR scan.

Video

Video available at www.sciencedirect.com

Segmentation Protocol

Each pair of baseline and postresection 7-T MRIs of each group was processed using the software 3D Slicer 4.10.2 (https://www.slicer.org/wiki/CitingSlicer).[29] The N4ITK bias field correction filter was used to normalize the signal inhomogeneity in each volume, which was particularly necessary for volumes of group 2 because of gadolinium hyperintensity. This image-filtering process does not require previous tissue classification.[30,31] After filtering, a combination of manual and semiautomatic segmentation methods was performed to assess the volumetric differences between baseline and postresection MRIs of calf hemispheres. Tissue types were defined as cerebral cortex, cerebral white matter, and artificial tumor; each tissue type was assigned a specific segment. Additional segments included fiducials and air. Each segment was assigned a specific color code, which was consistent across all MR volumes. The segmentation process was divided in 2 parts. First, white matter tracts were manually contoured by hand for improved accuracy. Image contrast was adjusted throughout the white matter segmentation process to highlight different sections of white matter tracts, such as borders between gray and white matter or white matter tracts directly adjacent to hyperintense tumor. Once white matter tracts were manually segmented, gray matter regions were segmented manually with level tracing around the white matter segment. Tumors were then automatically segmented

using the Otsu thresholding method.[25] For each brain volume, 20–30 slices were individually segmented, after which a semiautomatic growing seed function[24] was used to extend the segmentations to all slices. Air and ventricles were then automatically segmented using the Otsu thresholding method[25] and removed from the final segmentation. For greater anatomic accuracy, median smoothing with a 0.50-mm kernel size (3 × 3 × 3 pixels) was applied for white matter segments and gray matter segments.

Registration

Once segmentation was performed, postresection segmented images were registered on to the matching baseline segmented images to visualize the geographic location at which resection occurred. This registration was performed using the 3D Slicer extension "Segmentation registration."[32] The baseline segmentation and image were kept fixed as the matching postresection segmentation and image were displaced and deformed such that relevant anatomic landmarks from these brains matched their counterparts on the baseline brain. To account for deformation, several baseline brains had fiducials inserted to help in defining landmarks for registration. Registration occurred in multiple steps. First, when present, fiducials were registered using a rigid transformation of the postresection images. Second, if necessary, the postresection segmentation and image underwent another rigid transformation using white matter as the moving segments. If the postresection shape of the brain was significantly different from baseline on visual inspection, cerebral cortex underwent a deformable transformation. For each of the segments previously mentioned, registration was performed only once to reduce the amount of deformation of the postresection segment. After registration, a region of interest (ROI) was delimitated around the resected and operated regions to define the boundaries for the extraction of volumetric information. ROI delineation varied across brain hemispheres depending on the level of deformation of each hemisphere. In group 1 hemispheres, the ROIs were concentrated around the resection sites. In group 2 hemispheres, because the injection of the alginate artificial tumor caused deformation of adjacent brain structures, the ROIs were expanded to encompass the tumor and its immediate surroundings. In brain 3 of group 2, the deformation was such that the ROI encompassed the entire section of the brain containing the tumor.

Quantification of Normal Brain Tissue Removed

In the 3 group 1 hemispheres, predetermined segments of brain tissue were removed after the baseline scan, which was followed by a postresection scan. Quantitative information of each segment was available in the form of tables containing the segments statistics for each volume. Each table contained 2 sets of information: the segment statistics for the entire volume and the segment statistics for the region within the boundaries of the ROI. These tissue volumes were reported in milliliters. Differences in tissue volume between baseline and postresection images were calculated based on the segment statistics for each ROI. A linear model was created and used to predict the weight (in grams) of the removed tissue based on the tissue volume removed derived from the 7-T MRIs segmentation and registration results (Figure 3).

Quantification of Tumor and Gray and White Matter Tissue Resected

All volumes are reported in milliliters. In a calf hemisphere without the presence of a tumor after image segmentation and registration, the total baseline volume (ROI) was composed of total gray matter volume (N_g) and total white matter volume (N_w), which may be represented as:

$$ROI = N_g + N_w \quad (1)$$

In group 2, after image segmentation and registration, an ROI on the baseline scan containing the tumor was outlined (Figure 4A). The total baseline ROI volume is composed of total gray matter volume (N_g), total white matter volume (N_w), and tumor volume (N_t) Therefore, the total ROI volume which contains the tumor may be considered as:

$$ROI = N_g + N_w + N_t \quad (2)$$

The subpial removal for tumor involves resection of overlying gray and surrounding white matter along with the tumor amount removed. On the postresection images, the previously identified ROI on the baseline scan is composed of residual gray matter volume ($N_{g'}$), residual white matter volume ($N_{w'}$), residual tumor volume ($N_{t'}$), and total resected tissue volume (N_r), seen as empty space:

$$ROI = N_{g'} + N_{w'} + N_{t'} + N_r \quad (3)$$

The change in gray matter volume (ΔN_g) between the baseline and the postresection scan is the difference between the baseline gray matter volume (N_g) minus the residual gray matter volume ($N_{g'}$) after resection:

$$\Delta N_g = N_g - N_{g'} \quad (4)$$

The change in white matter volume (ΔN_w), which is the total volume of white matter resected, is the difference between the baseline white matter volume (N_w) minus the residual white matter volume ($N_{w'}$) after resection:

$$\Delta N_w = N_w - N_{w'} \quad (5)$$

The change in tumor volume (ΔN_t), which is the total volume of tumor resected, is the difference between the baseline tumor volume (N_t) minus the residual tumor volume after resection ($N_{t'}$):

$$\Delta N_t = N_t - N_{t'} \quad (6)$$

The total resected tissue volume (N_r) can be calculated from the following equation:

$$N_r = \Delta N_g + \Delta N_w + \Delta N_t \quad (7)$$

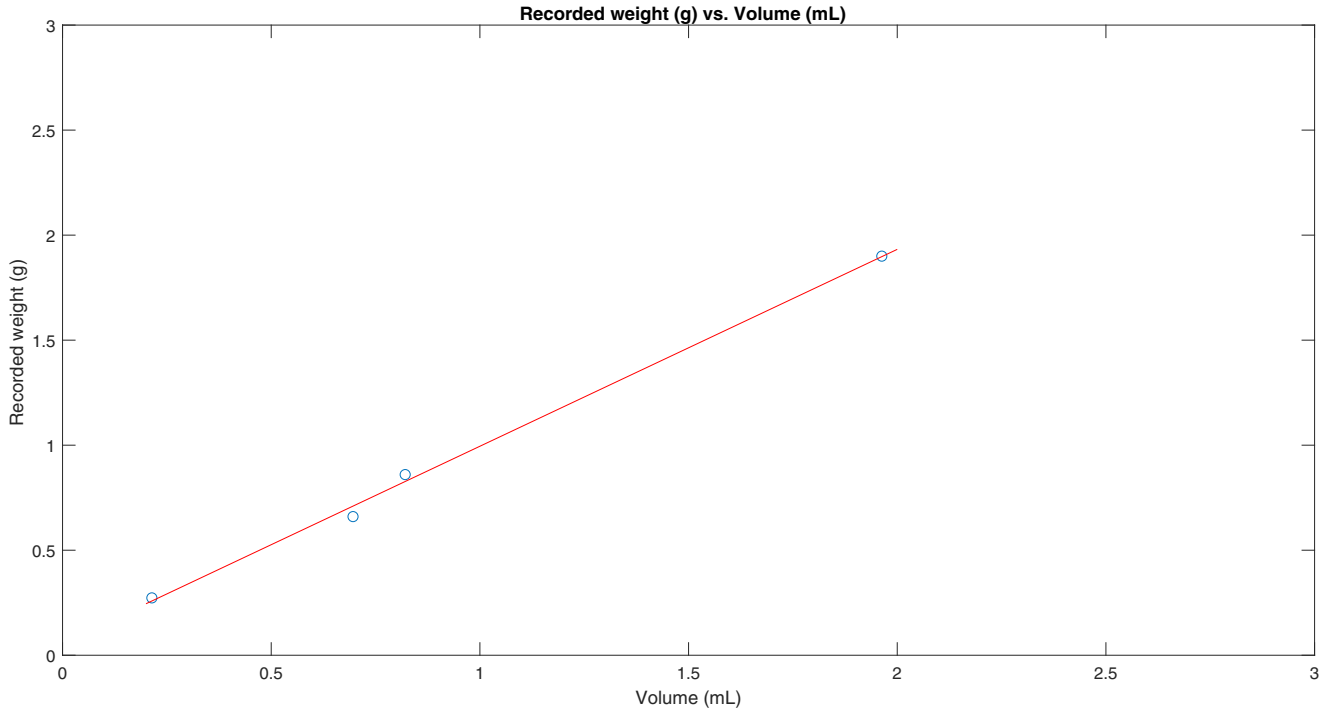

Figure 3. Recorded weights (grams) of resected brain segments versus their associated volumes (milliliters) determined from segmented images. Data points shown here are listed in **Table 1**. To show this quasi-linearity, a polynomial $p(x) = 0.9373\,x + 0.0576$ was fitted and plotted. A correlation coefficient of 0.9987 and an R^2 of 0.9974 between recorded weights and predicted weights were found, suggesting good correlation between the 2 measures.

Therefore, equation 7 allows for the calculation of the total resected tissue volume N_r during the procedure.

RESULTS

Quantification of Brain Tissue Removed

Six brain segments of increasing sizes were removed from the 3 calf hemispheres in group 1. Two small segments (0.17 and 0.54 g) could not be accurately identified on the postresection segmented images because of distortions associated with placing the postresection brain into the tube necessary for 7-T MRI. Four brain segments could be assessed (**Table 1**). Linear fitting of the data yielded a predictive model $p(x) = 0.9373\,x + 0.0576$. A correlation coefficient of 0.9987 and a coefficient of determination (R^2) of 0.9974 were established. The polynomial model can predict up to 99.74% of the variance in recorded weights (**Figure 3**). Volumetric data in milliliters of tissue removed when comparing baseline and postresection segmented images were analyzed using the developed polynomial model and the predicted error ranged from 0.11% to 7.58% (**Table 1**). These results suggest that the 7-T MRI techniques outlined can accurately predict small brain segment removals when deformation between baseline and postresection segmented images is not too significant. When the ROI on the postresection scan can be accurately delineated, the polynomial model can determine the brain tissue weights when larger amounts of brain are removed.

Quantification of Brain Tumor Removed

Four calf hemispheres were injected with alginate tumor ranging from 0.5 to 1.5 mL (**Table 2**). The alginate tumors were easily identified on the baseline coronal 7-T MRIs and segmented coronal images because of the presence of gadolinium (**Figure 4**). Postresection sagittal segmented images showed complete tumor removal in 3 of 4 tumors studied (**Figure 5**). The coronal and sagittal segmented images of the baseline scan show the presence of the injected alginate tumor in the gray matter gyrus (**Figures 4** and **5**). The area of tissue resection, involving gray matter, white matter, and tumor can be appreciated when comparing the detailed baseline and postresection coronal and sagittal segmentation images available. Injection of increased milliliters of alginate was associated with tumors of increased volume (**Table 2**). Baseline segmented sagittal images showed tumors of irregular form and different shapes (**Figure 5A**, **C**, **E**, and **G**). In brain 1, the tumor resection was subtotal; little gray matter overlying the tumor seemed to have been resected (**Figure 5B**). In postresection sagittal segmented images of brains 2 and 3, the overlying gray matter and a portion of white matter have been removed during the resection (**Figure 5D** and **F**). In the postresection image of brain 3 outlined in **Figure 5F**, the subpial gray matter resection seems incomplete, leaving irregular areas of gray matter in the resection cavity. In **Figure 5H**, the postresection cavity of brain 4 is severely compressed, leaving no resection cavity and thus preventing an

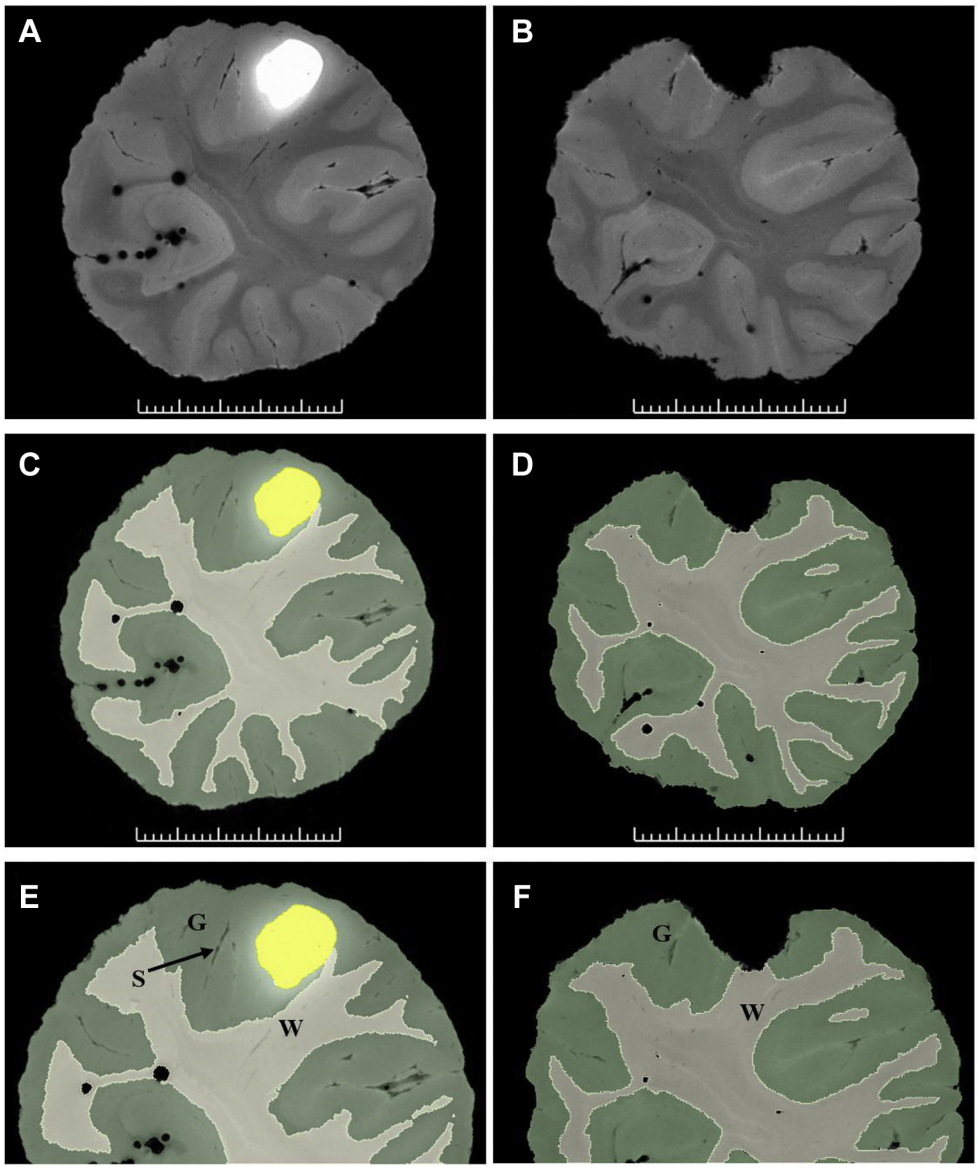

Figure 4. Coronal 7-T magnetic resonance images of calf brain hemisphere containing alginate tumor (group 2, calf brain hemisphere 2). (**A**) Baseline enhancing tumor (scale bar, 25 mm). (**B**) Postresection image after subpial gyral and tumor resection (scale bar, 25 mm). (**C**). Baseline segmented image of enhancing tumor (scale bar, 25 mm). (**D**) Postresection segmented image after subpial gyral and tumor resection (scale bar, 25 mm). (**E**) Detailed view of baseline enhancing tumor with compressed gray matter gyrus (*G*), displaced gyral sulcus (*S, arrow*) and white matter (*W*). (**F**) Detailed view of segmented image after subpial resection of overlying gyrus and tumor resection, showing the re-expanded intact adjacent gray matter gyrus with sulcus along with resection of white matter.

assessment of baseline gray (N_g) and white (N_w) matter removed tissue using our registration method. The ROI on a baseline coronal segmented image of a calf brain hemisphere containing an irregular tumor is delineated (Figure 6A). Both gray (N_g) and white (N_w) matter tissues are outlined in a detailed coronal segmented view of the ROI in which no tumor is present (Figure 6B). A baseline coronal segmented image of the ROI containing a complex irregular tumor is also shown (Figure 6C). Gray (N_g) and white matter (N_w) along with tumor (N_t) are outlined. On the postresection segmented coronal image, residual gray matter ($N_{g'}$) and residual white matter ($N_{w'}$) along with the residual tumor regions ($N_{t'}$)in the equivalent ROI location as on the postresection image can be identified (Figure 6D). An area of resected tissue can also be identified as

Table 1. Removed Brain Tissue Weights of 6 Segments from 3 Calf Brain Hemispheres

	Segments					
	1	2	3	4	5	6
Recorded weight (g)	0.17	0.27	0.54	0.66	0.86	1.9
Volume (mL)	—	0.214	—	0.696	0.821	1.963
Predicted weight (g)	—	0.258	—	0.710	0.827	1.898
Percent error $\left(\left\|\frac{\text{predicted} - \text{actual}}{\text{actual}}\right\| \times 100\%\right)$	—	4.44	—	7.58	3.84	0.11

Volumes derived from analysis of segmented images (mL) and predicted weights (g) along with percent error were computed based on the polynomial model *p(x)* as detailed in Figure 3.

empty space along with what seems to be tissue injury to gray matter and white matter structures involving adjacent gyri.

Calculation of Total Resected Tumor

In 3 of 4 calf hemispheres containing tumors that were operated on, 100% of the tumor was removed because no residual tumor could be visualized on the postresection images (Table 2). In the experiment in which postresection residual tumor was seen (brain 1), equation 6 was used to calculate the change in tumor volume (ΔN_t) between the baseline and after resection. This calculation was possible because the baseline and postresection ROI could be accurately aligned and the baseline tumor volume (N_t), residual tumor volume after resection ($N_{t'}$) and total volume of resected tumor (ΔN_t) could be calculated (Table 2). These results show that 56.5% of the tumor was resected, with 43.5% of residual tumor still present after tumor resection on the postresection images (Table 2).

Table 2. Injected Alginate Tumor Volumes and Gray Matter, White Matter, and Tumor Volumes in Region of Interest from 4 Calf Brain Hemispheres

	Calf Brain Hemisphere			
	1	2	3	4
Volume of injected alginate tumor (mL)	0.5	0.5	1.0	1.5
Volume of alginate tumor N_t inferred from 7-T magnetic resonance images (mL)	0.421	0.838	0.902	1.428
Tumor length (mm)	17.850	15.800	23.300	24.750
Baseline gray matter within ROI N_g (mL)	14.634	18.535	25.300	—
Baseline white matter within ROI N_w (mL)	7.848	6.037	14.049	—
Baseline ROI volume (mL)	22.903	25.410	40.251	—
Postresection tumor volume $N_{t'}$ (mL)	0.183	0	0	0
Resected tumor volume ΔN_t (mL)	0.238	0.838	0.902	1.428
Resected tumor volume (%)	56.5	100	100	100
Residual tumor volume (%)	43.5	0	0	0
Resected gray matter volume ΔN_g (mL)	0.145	1.968	5.901	—
Resected white matter volume ΔN_w (mL)	0.141	0.478	0.534	—
Ratio of gray matter resected to white matter resected	1.03:1	4.12:1	11.05:1	—
Total resected tissue volume N_r (mL)	0.524	3.284	7.337	—

Volumes in mL were derived from segmented baseline and postresection images. The baseline ROI volume in mL was composed of gray matter (N_g), white matter (N_w) and tumor (N_t). The postresection ROI volume was composed of residual gray matter ($N_{g'}$), residual white matter ($N_{w'}$), residual tumor ($N_{t'}$) and total resected tissue (N_r). The changes in gray matter (ΔN_g), in white matter (ΔN_w) and in tumor (ΔN_t) volumes in mL were calculated between baseline and postresection segmented ROI images. Adding these values allowed the calculation of total resected tissue (N_r). Percentage tumor resected and residual tumor volumes, tumor lengths, and total gray/total white matter ratios were also calculated. Percentage tumor resected and residual tumor volumes were calculated based on the volume of injected alginate tumor inferred from 7-T magnetic resonance images.
ROI, region of interest.

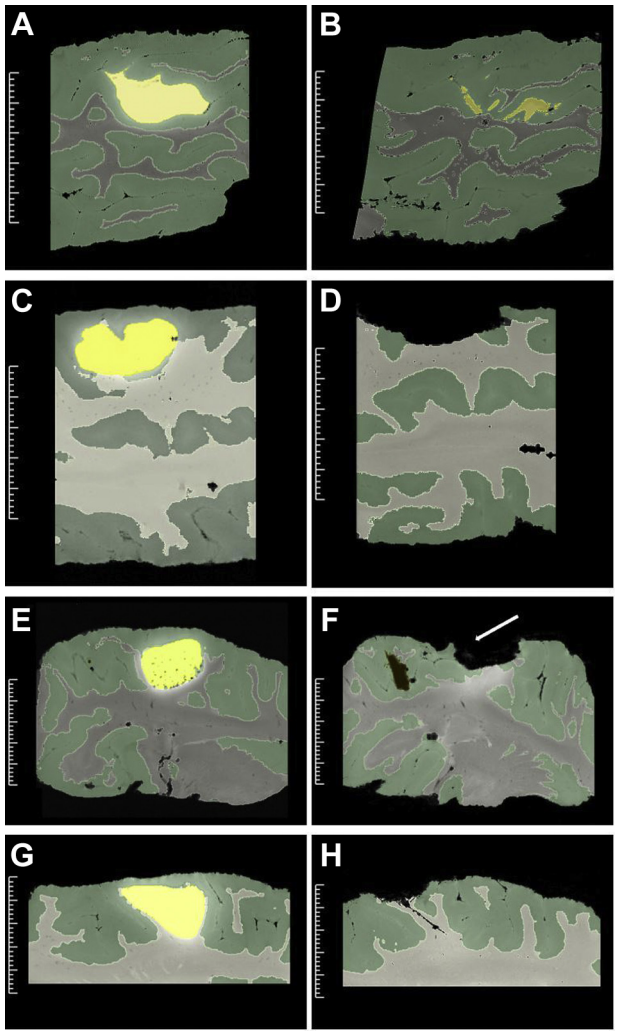

Figure 5. Sagittal 7-T magnetic resonance images of calf brain hemisphere containing alginate tumors, group 2. (**A**) Baseline segmented sagittal image of irregular tumor in calf brain hemisphere 1 (scale bar, 25 mm). (**B**) Postresection segmented sagittal image of brain hemisphere 1 after subpial gyral and tumor resection, showing subtotal resection with residual tumor (scale bar, 25 mm). (**C**) Baseline segmented sagittal image of tumor in calf brain hemisphere 2, showing an elongated irregular tumor (scale bar, 25 mm). (**D**) Postresection segmented sagittal image of brain hemisphere 2 after subpial gyral and tumor resection, showing resection of overlying gyral gray matter along with complete tumor resection (scale bar, 25 mm). (**E**) Baseline segmented sagittal image of tumor in calf brain hemisphere 3, showing an oval tumor (scale bar, 25 mm). (**F**) Postresection segmented sagittal image of brain hemisphere 3 after subpial gyral and tumor resection, showing resection of overlying gyral gray matter and white matter tract. Residual regions of gray matter tissue irregularities in the resection cavity (*arrow*) consistent with residual gray matter and gray matter injury are also apparent (scale bar, 25 mm).(**G**) Baseline segmented sagittal image of tumor in calf brain hemisphere 4, showing the presence of tumor in the white matter (scale bar, 25 mm). (**H**) Postresection segmented sagittal image of brain hemisphere 4 after subpial gyral and tumor resection, showing collapse of the resection cavity (scale bar, 25 mm).

Calculation of Total Gray and White Matter Resected

In 3 of 4 calf hemispheres with tumors, the baseline gray (N_g) and white matter volume (N_w) within their respective ROI could be calculated (Table 2). In these 3 tumors, it was possible to calculate residual gray ($N_{g'}$) and residual white matter ($N_{w'}$) present in the ROI of the postresection images (Table 2). In brain hemisphere 4, the baseline and postresection images could not be accurately aligned because the resection cavity was compressed (Figure 5G and H). The ability to accurately calculate residual gray ($N_{g'}$) and residual white matter ($N_{w'}$) volumes present on the postresection images for 3 tumors allowed for the calculation of change in gray (ΔN_g) and white matter volume (ΔN_w), and resected gray and white matter, respectively, on the postresection images (Table 2). It was the expectation that more gray than white matter would be removed during the subpial resection of tumors and the gray/white matter ratios seemed consistent with that expectation (Table 2).

Calculation of Total Tissue Resected

For 2 tumors studied in which the tumor was completely removed ($\Delta N_t = 0$) and for the incompletely resected tumor, the total tumor resected volume (ΔN_t) was successfully calculated. Because it was also possible to calculate residual gray matter ($N_{g'}$), residual white matter, ($N_{w'}$), and residual tumor (ΔN_t) volumes present on the postresection images, the total volume of tissue removed (N_r) during the subpial resection could be calculated using equation 7. The total tissue resected ranged from 0.524 to 7.337 mL (Table 2).

Postresection Structural Integrity Analysis of Gray and White Matter Tracts

The registration process of the baseline and postresection 7-T MRIs provided structural information on the integrity of gray matter gyri and white matter tracts in the vicinity of the tumor before and after tumor resection. By matching each point on the postresection segmented image with its analog on the baseline segmented image using the Slicer extension "Segmentation registration,"[32] it was possible to evaluate the differences between both images after they were automatically registered by the software (Figure 5). On the baseline sagittal segmented images provided, the injected alginate resulted in irregular tumors within and covered by the overlying gray matter gyrus (Figure 5A, C, E, G). In some postresection segmented images, irregularities in the residual gray matter tissue can be visualized, which is consistent with incomplete resection of overlying gray matter and gray matter injury (Figure 5F and 6D). Residual tumor tissue in this model can be identified and easily quantitated on postresection images (Figures 5 and 6). Although fiducials were placed on only 1 brain in group 2, their presence improved baseline and postresection image alignment by acting as landmarks that could be easily recognized and registered. A video containing scrolling coronal baseline and postresection images is provided for brain 1 of group 2 and brain 3 of group 2 (Video 1). The video can be used to provide the learner with further information on surgical performance. Violation of the surgical pial boundaries and damage to the adjacent gyrus are

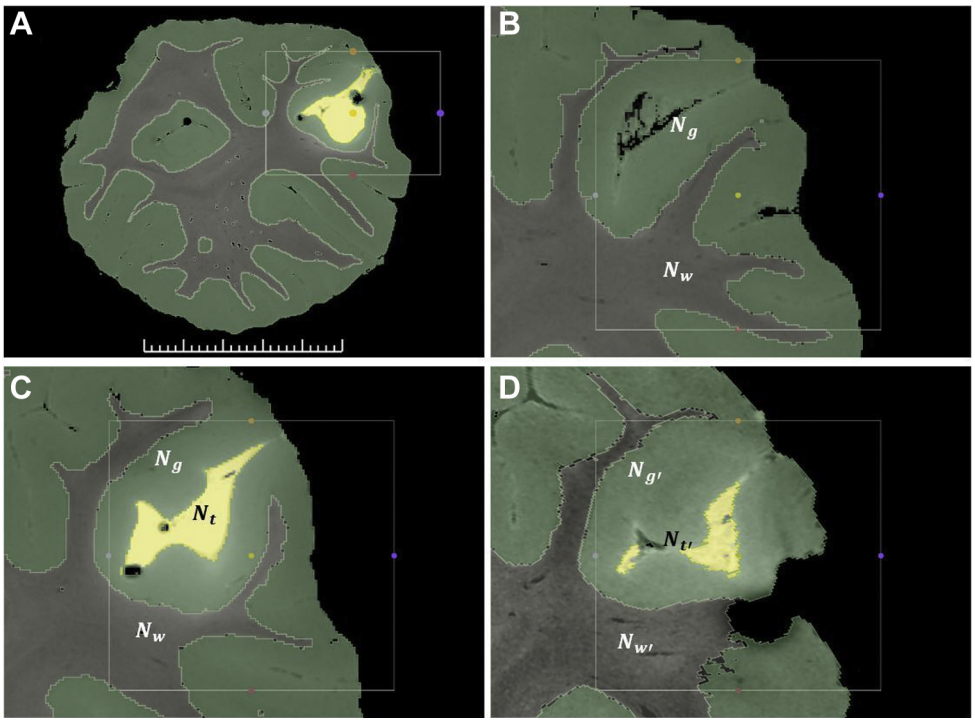

Figure 6. Coronal 7-T magnetic resonance images of segmented calf brain hemisphere (group 2, calf brain hemisphere 1) labeled with quantifiable variables. (**A**) Baseline coronal segmented image of calf brain hemisphere (scale bar, 25 mm) containing irregular tumor outlined within an outlined region of interest (ROI). (**B**) Detailed view of the segmented image with ROI in which no tumor is visualized with quantifiable gray (N_g) and white matter (N_w) tissue regions. (**C**) Detailed view of baseline segmented image with ROI and quantifiable gray (N_g) and white matter (N_w) tissue along with quantifiable tumor (N_t). (**D**) Detailed view of the postresection segmented image with ROI and quantifiable residual gray ($N_{g'}$) and residual white matter ($N_{w'}$) along with residual tumor ($N_{t'}$).

particularly apparent when both baseline and postresection segmented MRIs are put side by side for comparison.

Baseline and Postresection 3D Reconstruction Views

Using the information available on the segmented baseline and postresection images, it is possible to develop 3D reconstructions of the calf brain containing the tumor and postresection residual tumor (Figure 7). These images can provide further information related to the surface structure of the resection cavity and the 3D structure of the tumor within the calf brain both before and after resection; in the case of brain 1 of group 2, this sort of 3D view allowed the visualization of the residual tumor remaining after the subtotal resection (Figure 7).

DISCUSSION

Summary

This pilot study was carried out as a proof of concept that the combination of using a brain tumor resection model and segmented 7-T MRIs is feasible and has the potential to aid in understanding and evaluating neurosurgical performance. We were able to fulfill our aims of quantitating brain tissue removal, alginate brain tumor resected, and normal gray and white matter resected along with total tissue resected after subpial resection in a calf brain model.

Quantification of Brain Tissue Removed

The image analysis based on segmented 7-T MRIs used in this study can be used with the developed polynomial model to accurately predict small brain segment removals if brain deformation between baseline and postresection images is minimal. Significant deformation of anatomic structures in the baseline and postresection images prevents the registration of the 2 images, thus preventing the calculation of the difference in tissue volumes between the 2 images. Another limiting factor is the size of the removed piece of tissue. Smaller pieces cannot be accurately analyzed because they can easily be mistaken for brain surface deformation. The polynomial model can determine the brain tissue weights in grams when larger amounts of brain are removed. Further investigation needs to be performed to increase our ability to measure smaller quantities of brain tissue removed.

Alginate Tumor Model and Quantitative Analysis of Tissue Resections

Although attempts were made to provide the ex vivo alginate tumor model used with color and tumor stiffness characteristics

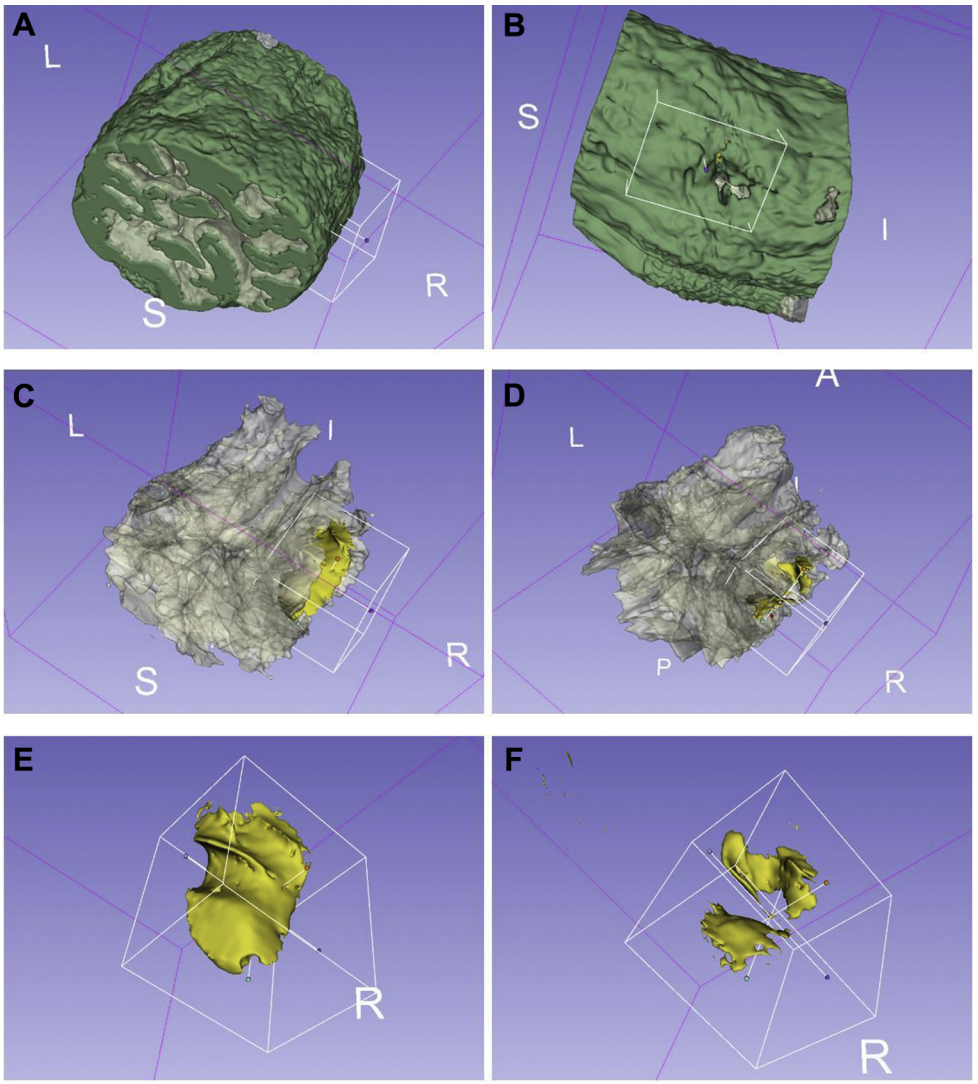

Figure 7. Baseline and postresection three-dimensional (3D) reconstruction views of calf brain hemisphere containing alginate tumor (group 2, calf brain hemisphere 1). (**A**) Baseline 3D reconstruction of calf brain 1 showing region of interest (ROI) containing the tumor. (**B**) Reconstructed 3D postresection surface view showing that very small amounts of overlying gray matter were removed during tumor resection. (**C**) Reconstructed baseline 3D view containing the ROI in which gray matter has been removed to allow visualization of white matter (*white*) and tumor (*yellow*). (**D**) Reconstructed postresection 3D view containing the ROI outlining the position and shape of the residual tumor (*yellow*). (**E**) Reconstructed baseline 3D view containing the ROI in which the gray and white matter have been removed, allowing visualization of the irregular shape of the tumor (*yellow*). (**F**) Reconstructed postresection 3D view containing the ROI in which the gray and white matter have been removed, allowing visualization of the 2 areas of residual tumor (*yellow*). The *white box,* which outlines the ROI, was kept constant between the baseline and postresection 3D views. A, anterior; P, posterior; R, right; L, left; S, superior; I, inferior.

associated with human tumors, the model does not reproduce the multiple consistencies and bleeding associated with human glial tumors. Therefore, our studies are not able to assess the influence of these factors of resection technique. The alginate tumor hydrodissection injection into calf brain cortical gray matter resulted in a variety of tumor shapes, necessitating careful delineation of the ROI on the baseline and postresection images (Figure 5).The alginate tumor model and the segmentation and registration 7-Tesla MRI techniques utilized in this study allowed quantitative assessment of all 4 tumor volumes (N_t) and 3 out of 4 gray matter (N_g) and white matter (N_w) volumes within ROI outlined on baseline scans. The quantitation of residual gray matter ($N_{g'}$) and residual white matter ($N_{w'}$) along with the residual tumor ($N_{t'}$) in the equivalent ROI location after resection is

important to allow calculation of change in gray matter (ΔN_g), change in white matter (ΔN_w)and change in tumor (ΔN_t). Using equation 7, the value for total resected tissue (N_r) can be obtained. This procedure is possible only if accurate alignment of baseline and postresection images can be achieved, which was accomplished in 3 of 4 tumors studied. Although only a small series, 4 of 7 calf hemispheres studied contained fiducials. There seemed to be an improvement in registration of baseline and postresection segmented images when fiducials were present. Accurate registration was not possible for the largest tumor in the series because of the infolding and collapse of the resection cavity during placement in the MRI coil (**Figure 5**). This situation suggested that larger resection cavities tend to be more compressible after being placed in the coil. Conceptually, filling the resection cavity after the completion of the procedure with an incompressible material that is not visible on MRI would result in lesser deformation, allow improved alignment, and increase the ability to find all 3 variables necessary to solve equation 7. Studies are ongoing to evaluate possible materials that could perform this function.

Educational Opportunities: Combining Virtual Reality and Ex Vivo Models

Ex vivo models have been developed to aid in the assessment of neurosurgical technical skills. The ex vivo bovine model used in these studies is not an exact replicate for the human brain regarding size and convolutional surface appearance and should not be considered a substitute for the detailed anatomic studies involving cadaveric models. However, ex vivo models do provide new methods to quantitate trainees' technical skills and different educational opportunities for learners. MRI has not been previous used to assess psychomotor bimanual performance in these model systems. Preresection and postresection imaging, whether MR or computed tomography,[33] is available for patients undergoing operation for tumor resection but the ability to accurately quantitate gray and white matter removal in these procedures is difficult. The ability to use this tumor model in combination with 7-T MRI provides an opportunity to increase the granularity of data obtainable from operative procedures. Our group has used high-fidelity virtual reality simulators with haptic feedback to develop a model for bimanual psychomotor surgical performance[8] and for quantitative assessment of expert performance.[5,34] Present studies are focused on developing intelligent tutoring systems using machine learning[15] and artificial neural networks[35] for assessment and training of surgical performance[36] along with the development of complex neurosurgical scenarios for use in these tutoring sytems.[37,38] The ability to compare expert performance on surgical virtual reality simulators to that in controlled operating room environments would advance both the understanding of surgical expertise and the ability to train learners to the mastery level using these intelligent tutoring systems.[36,39] The combination of developing standardized alginate tumor and epilepsy models using the ex vivo calf brain model outlined in this communication along with segmentation and registration MRI technologies allows for future studies in skills transfer between virtual reality simulators and the operating room. These investigations would be able to focus not only on amount of tumor tissue resected but also on quantity of normal gray matter and white matter tracts resected, the method of resection, and the tissue injury to adjacent areas.

Limitations

Although this is to our knowledge the first study that attempts to provide a quantitative method of analysis on an artificial tumor model obtained from a 7-T MRI scanner, there are limitations. First, the polynomial model developed using brain sections involving both gray and white matter was limited and needs to be expanded. Our polynomial model was based on 4 brain segments; further studies with different sizes of brain tissue removed must be carried out to increase the accuracy and predictive power of the model. Second, to quantitate residual gray and white matter in the postresection segmented images, methods to prevent infolding of the resection cavity need to be developed to avoid being unable to register preresection and postresection segmented MRIs such as in the case of brain 4 (**Figure 5H**). Studies are under way to address this issue. Third, this model does not allow for an assessment of vascular injury but methods to perfuse the ex vivo calf brain hemispheres are being explored. Fourth, regarding segmentation, although manual segmentation remains the gold standard, it induces a range of variability in accuracy that may affect the quality of the segmentations.[16,18,19] Variability may result from user factors and signal inhomogeneity of the volume despite the filtering process, particularly when same tissue types show residual noise.[40] Manual segmentation requires a significantly higher amount of time compared with automatic methods, which may not be adapted to the clinical setting. Choosing the proper ROI after segmentation and registration is also time consuming and requires expertise. For instance, the processing of brain 4 was not possible not only because the postresection cavity collapsed on itself but also because only half of the brain was scanned, thus omitting important brain landmarks that could have been used to perform registration. The choice of FOV for this brain was made with the idea that scanning the half of the brain that contains the tumor would be easier than scanning the whole brain. No atlas or database on calf brain exists, which makes the development of an automated segmentation pipeline difficult. The number of calf brain hemispheres used in this pilot study was small. However, these investigations functioned as a proof of concept and outlined important issues that need to be addressed to improve future studies. Only a few institutions have access to animal 7-T MRI units, limiting the number of research centers that can carry out these types of investigations. Studies using human 7-T MRI to quantitate operative performance may also find these studies useful.

CONCLUSIONS

This pilot study was carried out as a proof of concept to show the feasibility of using brain tumor models combined with 7-T MRI technology to quantitate brain tumor resection along with normal gray matter, normal white matter, and total tissue resected after subpial resection procedures in a calf brain ex vivo tumor model.

The ability to use tumor models in combination with 7-T MRI provides an opportunity to increase the granularity of data obtained from operative procedures and improve the assessment and training of learners.

CRediT AUTHORSHIP CONTRIBUTION STATEMENT

Dan Huy Tran: Conceptualization, Methodology, Software, Validation, Formal analysis, Investigation, Resources, Data curation, Writing - original draft, Writing - review & editing, Visualization, Supervision, Project administration. **Alexander Winkler-Schwartz:** Conceptualization, Methodology, Resources, Writing - review & editing, Funding acquisition. **Marius Tuznik:** Investigation, Data curation, Writing - review & editing. **Houssem-Eddine Gueziri:** Conceptualization, Methodology, Software, Investigation. **David A. Rudko:** Methodology, Investigation, Software, Resources, Writing - review & editing, Supervision. **Aiden Reich:** Conceptualization, Writing - review & editing. **Recai Yilmaz:** Conceptualization, Methodology. **Bekir Karlik:** Conceptualization, Methodology. **D. Louis Collins:** Methodology, Software, Writing - review & editing. **Adrian Del Maestro:** Methodology. **Rolando Del Maestro:** Conceptualization, Methodology, Resources, Writing - review & editing, Supervision, Funding acquisition.

ACKNOWLEDGMENTS

The authors would like to thank Dr. Carlo Santaguida, Department of Neurology and Neurosurgery, Montreal Neurological Institute and Hospital, McGill University for his help with this project.

REFERENCES

1. Sealy WC. Halsted is dead: Time for change in graduate surgical education. *Curr Surg*. 1999;56:34-39.
2. Brightwell A, Grant J. Competency-based training: who benefits? *Postgrad Med J*. 2013;89:107-110.
3. Silbergeld D, Hebb A, Yang T. The sub-pial resection technique for intrinsic tumor surgery. *Surg Neurol Int*. 2011;2:180.
4. Valli D, Belykh E, Zhao X, et al. Development of a simulation model for fluorescence-guided brain tumor surgery. *Front Oncol*. 2019;9:748.
5. Azarnoush H, Alzhrani G, Winkler-Schwartz A, et al. Neurosurgical virtual reality simulation metrics to assess psychomotor skills during brain tumor resection. *Int J Comput Assist Radiol Surg*. 2014;10:603-618.
6. Azarnoush H, Siar S, Sawaya R, et al. The force pyramid: a spatial analysis of force application during virtual reality brain tumor resection. *J Neurosurg*. 2017;127:171-181.
7. Bugdadi A, Sawaya R, Olwi D, et al. Automaticity of force application during simulated brain tumor resection: testing the Fitts and Posner model. *J Surg Educ*. 2018;75:104-115.
8. Sawaya R, Alsideiri G, Bugdadi A, et al. Development of a performance model for virtual reality tumor resections. *J Neurosurg*. 2019;131:192-200.
9. Sawaya R, Bugdadi A, Azarnoush H, et al. Virtual reality tumor resection: the force pyramid approach. *Oper Neurosurg (Hagerstown)*. 2018;14:686-696.
10. Winkler-Schwartz A, Bajunaid K, Mullah MAS, et al. Bimanual psychomotor performance in neurosurgical resident applicants assessed using NeuroTouch, a virtual reality simulator. *J Surg Educ*. 2016;73:942-953.
11. Jensen Ang WJ, Hopkins ME, Partridge R, et al. Validating the use of smartphone-based accelerometers for performance assessment in a simulated neurosurgical task. *Neurosurgery*. 2014;10:57-65.
12. Alotaibi FE, AlZhrani GA, Mullah MA, et al. Assessing bimanual performance in brain tumor resection with NeuroTouch, a virtual reality simulator. *Neurosurgery*. 2015;11:89-98.
13. Holloway T, Lorsch ZS, Chary MA, et al. Operator experience determines performance in a simulated computer-based brain tumor resection task. *Int J Comput Assist Radiol Surg*. 2015;10:1853-1862.
14. Bajunaid K, Mullah MA, Winkler-Schwartz A, et al. Impact of acute stress on psychomotor bimanual performance during a simulated tumor resection task. *J Neurosurg*. 2017;126:71-80.
15. Winkler-Schwartz A, Yilmaz R, Mirchi N, et al. Machine learning identification of surgical and operative factors associated with surgical expertise in virtual reality simulation. *JAMA Network Open*. 2019;2:e198363.
16. Despotović I, Goossens B, Philips W. MRI segmentation of the human brain: challenges, methods, and applications. *Comput Math Methods Med*. 2015;2015:1-23.
17. Roy S, Bandyopadhyay SK. Detection and quantification of brain tumor from MRI of brain and it's symmetric analysis. *Int J Inf Commun Technol*. 2012;2.
18. Abdallah MB, Blonski M, Wantz-Mézières S, Gaudeau Y, Taillandier L, Moureaux J-M. *Statistical evaluation of manual segmentation of a diffuse low-grade glioma MRI dataset. In: 2016 38th Annual International Conference of the IEEE Engineering in Medicine and Biology Society (EMBC)*. Piscataway, NJ: Institute of Electrical and Electronics Engineers; 2016:4403-4406.
19. Veeraraghavan H, Miller JV. *Active learning guided interactions for consistent image segmentation with reduced user interactions. In: 2011 IEEE International Symposium on Biomedical Imaging: From Nano to Macro*. Piscataway, NJ: Institute of Electrical and Electronics Engineers; 2011:1645-1648.
20. Pichon E, Tannenbaum A, Kikinis R. A statistically based flow for image segmentation. *Med Image Anal*. 2004;8:267-274.
21. Holz D, Behnke S. Fast range image segmentation and smoothing using approximate surface reconstruction and region growing. *Intelligent Autonomous Systems*. 2013;12:61-73.
22. Kim YJ, Lee SH, Park CM, Kim KG. Evaluation of semi-automatic segmentation methods for persistent ground glass nodules on thin-section CT scans. *Healthc Inform Res*. 2016;22:305-315.
23. Tingelhoff K, Moral AI, Kunkel ME, et al. *Comparison between manual and semi-automatic segmentation of nasal cavity and paranasal sinuses from CT images. In: 2007 29th Annual International Conference of the IEEE Engineering in Medicine and Biology Society*. Piscataway, NJ: Institute of Electrical and Electronics Engineers; 2007:5505-5508.
24. Adams R, Bischof L. Seeded region growing. *IEEE Trans Pattern Anal Mach Intell*. 1994;16:641-647.
25. Otsu N. A threshold selection method from gray-level histograms. *IEEE Trans Syst Man, Cybernetics*. 1979;9:62-66.
26. Winkler-Schwartz A, Yilmaz R, Tran DH, et al. Creating a comprehensive research platform for surgical technique and operative outcome in primary brain tumor neurosurgery. *World Neurosurg*. 2020;144:e62-e71.
27. Springer E, Dymerska B, Cardoso PL, et al. Comparison of routine brain imaging at 3 T and 7 T. *Invest Radiol*. 2016;51:469-482.
28. Trattnig S, Springer E, Bogner W, et al. Key clinical benefits of neuroimaging at 7 T. *NeuroImage*. 2018;168:477-489.
29. Fedorov A, Beichel R, Kalpathy-Cramer J, et al. 3D Slicer as an image computing platform for the Quantitative Imaging Network. *Magn Reson Imaging*. 2012;30:1323-1341.
30. Tustison N, Gee J. N4ITK: Nick's N3 ITK implementation for MRI bias field correction. *Insight J*. 2009:1-8.

31. Tustison NJ, Avants BB, Cook PA, et al. N4ITK: improved N3 bias correction. *IEEE Trans Med Imaging*. 2010;29:1310-1320.

32. Fedorov A, Khallaghi S, Sánchez CA, et al. Open-source image registration for MRI–TRUS fusion-guided prostate interventions. *Int J Comput Assist Radiol Surg*. 2015;10:925-934.

33. Grosch AS, Schroder T, Schroder T, Onken J, Picht T. Development and initial evaluation of a novel simulation model for comprehensive brain tumor surgery training. *Acta Neurochir (Wien)*. 2020; 162:1957-1965.

34. Alotaibi FE, AlZhrani GA, Sabbagh AJ, Azarnoush H, Winkler-Schwartz A, Del Maestro RF. Neurosurgical assessment of metrics including judgment and dexterity using the virtual reality simulator NeuroTouch (NAJD Metrics). *Surg Innov*. 2015;22:636-642.

35. Mirchi N, Bissonnette V, Ledwos N, et al. Artificial neural networks to assess virtual reality anterior cervical discectomy performance. *Oper Neurosurg (Hagerstown)*. 2020;19:65-75.

36. Mirchi N, Bissonnette V, Yilmaz R, Ledwos N, Winkler-Schwartz A, Del Maestro RF. The Virtual Operative Assistant: an explainable artificial intelligence tool for simulation-based training in surgery and medicine. *PLoS One*. 2020;15: e0229596.

37. Sabbagh AJ, Bajunaid KM, Alarifi N, et al. Roadmap for developing complex virtual reality simulation scenarios: subpial neurosurgical tumor resection model. *World Neurosurg*. 2020;139: e220-e229.

38. Ledwos N, Mirchi N, Bissonnette V, Winkler-Schwartz A, Yilmaz R, Del Maestro RF. Virtual reality anterior cervical discectomy and fusion simulation on the novel Sim-Ortho platform: validation studies. *Oper Neurosurg (Hagerstown)*. 2020;20:74-82.

39. Mirchi N, Ledwos N, Del Maestro RF. Intelligent tutoring systems: re-envisioning surgical education in response to COVID-19 [e-pub ahead of print]. *Can J Neurol Sci*. https://doi.org/10.1017/cjn.2020.202, accessed September 11, 2020.

40. Withey DJ, Koles ZJ. *Medical image segmentation: methods and software. In: 2007 Joint Meeting of the 6th International Symposium on Noninvasive Functional Source Imaging of the Brain and Heart and the International Conference on Functional Biomedical Imaging*. 2007:140-143.

Conflict of interest statement: This work was supported by the Franco Di Giovanni Foundation, the Montreal English School Board, the Montreal Neurological Institute and Hospital. A.W.-S. received a doctoral training grant for applicants with a professional degree of the Fonds de recherche du Québec—Santé (fund number 261422) and holds the Robert Maudsley Fellowship for Studies in Medical Education by the Royal College of Physicians and Surgeons of Canada.

Received 18 August 2020; accepted 27 December 2020

Citation: World Neurosurg. (2021) 148:e326-e339.
https://doi.org/10.1016/j.wneu.2020.12.141

Journal homepage: ***www.journals.elsevier.com/world-neurosurgery***

Available online: ***www.sciencedirect.com***

1878-8750/$ - see front matter